AFRL-VA-WP-TP-2004-304

FLIGHT TEST RESULTS OF AN ADAPTIVE GUIDANCE SYSTEM FOR REUSABLE LAUNCH VEHICLES

John D. Schierman, Neha Gandhi, Jason R. Hull, and David G. Ward

FEBRUARY 2004

Approved for public release; distribution is unlimited.

AIR VEHICLES DIRECTORATE
AIR FORCE RESEARCH LABORATORY
AIR FORCE MATERIEL COMMAND
WRIGHT-PATTERSON AIR FORCE BASE, OH 45433-7542

REPORT DOCUMENTATION PAGE

Form Approved
OMB No. 0704-0188

1. REPORT DATE *(DD-MM-YY)*	2. REPORT TYPE	3. DATES COVERED *(From - To)*
February 2004	Conference Paper Preprint	

4. TITLE AND SUBTITLE
FLIGHT TEST RESULTS OF AN ADAPTIVE GUIDANCE SYSTEM FOR REUSABLE LAUNCH VEHICLES

5a. CONTRACT NUMBER
F33615-01-C-3114

5b. GRANT NUMBER

5c. PROGRAM ELEMENT NUMBER
65502F

6. AUTHOR(S)
John D. Schierman, Neha Gandhi, Jason R. Hull, and David G. Ward

5d. PROJECT NUMBER
3005

5e. TASK NUMBER
40

5f. WORK UNIT NUMBER
LE

7. PERFORMING ORGANIZATION NAME(S) AND ADDRESS(ES)

Barron Associates, Inc.
1160 Pepsi Place, Suite 300
Charlottesville, VA 22901-0807

8. PERFORMING ORGANIZATION REPORT NUMBER

9. SPONSORING/MONITORING AGENCY NAME(S) AND ADDRESS(ES)

Air Vehicles Directorate
Air Force Research Laboratory
Air Force Materiel Command
Wright-Patterson Air Force Base, OH 45433-7542

10. SPONSORING/MONITORING AGENCY ACRONYM(S)
AFRL/VACA

11. SPONSORING/MONITORING AGENCY REPORT NUMBER(S)
AFRL-VA-WP-TP-2004-304

12. DISTRIBUTION/AVAILABILITY STATEMENT
Approved for public release; distribution is unlimited.

13. SUPPLEMENTARY NOTES
Conference paper to be presented at the AIAA Guidance, Navigation and Control Conference, Providence, RI, August 4, 2004. This paper was produced under a SBIR contract.

14. ABSTRACT
To enable autonomous operations in future Reusable Launch Vehicles (RLVs), reconfigurable control and adaptive guidance will often be required to facilitate recovery of the mission following a major anomalous event such as an effector failure. An adaptive guidance system that works in conjunction with a reconfigurable controller and an autonomous trajectory command reshaping algorithm is presented. The guidance law utilizes a backstepping architecture to generate pitch rate commands that drive the inner-loop control system. Under extreme failure conditions the control surfaces can saturate in an attempt to meet commanded moments. In these cases, the guidance feedback gains are reduced to preserve stability margins in the guidance loops. A case study is presented that shows the benefits of the guidance gain adaptation. Without adjusting the gains, the guidance loops go unstable, whereas stability is maintained with gain reduction.

15. SUBJECT TERMS
Adaptive Guidance, Reconfigurable Control

16. SECURITY CLASSIFICATION OF:			17. LIMITATION OF ABSTRACT:	18. NUMBER OF PAGES	19a. NAME OF RESPONSIBLE PERSON (Monitor)
a. REPORT	b. ABSTRACT	c. THIS PAGE			Dr. David Doman
Unclassified	Unclassified	Unclassified	SAR	22	19b. TELEPHONE NUMBER *(Include Area Code)* (937) 255-8451

Standard Form 298 (Rev. 8-98)
Prescribed by ANSI Std. Z39-18

FLIGHT TEST RESULTS OF AN ADAPTIVE GUIDANCE SYSTEM FOR REUSABLE LAUNCH VEHICLES

John D. Schierman, Neha Gandhi, Jason R. Hull, and David G. Ward

BARRON ASSOCIATES, INC.
1160 Pepsi Place, Suite 300
Charlottesville, VA 22901-0807
434-973-1215
schierman@bainet.com

ABSTRACT

To enable autonomous operations in future Reusable Launch Vehicles (RLVs), reconfigurable control and adaptive guidance will often be required to facilitate recovery of the mission following a major anomalous event such as an effector failure. An adaptive guidance system that works in conjunction with a reconfigurable controller and an autonomous trajectory command reshaping algorithm is presented. The guidance law utilizes a backstepping architecture to generate pitch rate commands that drive the inner-loop control system. Under extreme failure conditions the control surfaces can saturate in an attempt to meet commanded moments. In these cases, the guidance feedback gains are reduced to preserve stability margins in the guidance loops. A case study is presented that shows the benefits of the guidance gain adaptation. Without adjusting the gains, the guidance loops go unstable, whereas stability is maintained with gain reduction.

In addition, flight test results of the complete reconfigurable control/adaptive guidance system are presented for a simulated X-40A RLV. The Total In-Flight Simulator research aircraft was utilized to flight test the X-40A under a variety of failure conditions. This work was completed in conjunction with the Air Force Research Laboratory's Integrated Adaptive Guidance & Control (IAG&C) program.

1. INTRODUCTION

One of the overriding goals of NASA's *Next Generation Launch Technologies* efforts is to develop new launch systems and space transportation architectures that are significantly safer, more reliable and less costly. Recent interest in access to space has seeded similar goals for the Air Force. Both NASA and the Air Force have recognized that these goals must be accomplished in order for the U.S. to maintain its leadership role in space. To address the goal of increasing vehicle safety and reliability, there is now significant interest in reconfiguration technologies for the control and avionics systems of next generation *Reusable Launch Vehicles,* or *RLVs.* On-line reconfiguration can give the vehicle the capability to account for unexpected or unforeseen changes to the dynamics, aerodynamics, or control of the vehicle. Such changes may be due to, for example, control effector failures. However, RLVs typically do not possess the actuation redundancy or alternate control effectors seen in commercial or military aircraft, and this makes the reconfiguration task that much more challenging. Because of this, the reconfiguration problem will often involve not only the control of the vehicle, but also the guidance and the trajectory command functions as well.

A unique approach to the RLV on-line reconfiguration/adaptation problem is discussed herein. Along with a reconfigurable control system, this approach involves two main elements:

1. *Guidance gain adaptation:* An adaptive backstepping approach [1] has been developed to deliver commands to the inner-loop control system. Following an effector failure, information regarding control saturation and/or inner-loop bandwidth reduction is identified on-line and delivered to algorithms that adapt the feedback gains of the guidance law. Flight path stability is then maintained in the face of degraded maneuvering capabilities.

2. *On-line trajectory command reshaping:* Even with flight path stability maintained, the trajectory commands driving the guidance system may need to be continually reshaped on-line in order to achieve desired end conditions of the mission segment (e.g. on final approach, desired end conditions are characterized by a soft landing, at a certain runway touchdown point, at a certain flight speed). The approach discussed here is denoted as the *Optimum-Path-To-Go (OPTG)* algorithm [2]. Polynomial networks describing the "best" remaining path to the end of the mission segment are interrogated on-line at regular intervals to obtain the optimal trajectory commands, given the current state and "health" of the vehicle.

The work presented herein was jointly funded by both the Air Force Research Lab (AFRL) and NASA, Marshall Space Flight Center (MSFC). A detailed design of the adaptive guidance system and on-line trajectory command-reshaping algorithm was integrated with a reconfigurable control system designed by AFRL [3]. The demonstration platform for this development was Boeing's X-40A RLV, as shown in Figure 1. This is an unpiloted test bed vehicle with autonomous control and guidance. The X-40A is a technology demonstrator for its orbital counterpart, the X-37. The control effectors modeled for the X-40A were:

1. Left and right ruddervators: much like missile fin surfaces, these act as both pitch (asymmetric deflection) and yaw/roll (symmetric deflection) control effectors.

2. Left and right flaperons: these act as both lift generating devices (symmetric deflection) and as ailerons for roll control (asymmetric deflection).

3. Speedbrake: this is a surface on the top of the fuselage between the ruddervators, and can be deflected upward to 70 deg. It is nominally deflected to approximately 20 deg. so that the velocity can be controlled in both directions (reduce deflection to speed up, increase deflection to slow down). Under certain failure scenarios, the speedbrake can be employed to produce some pitching moment.

4. Bodyflap: this surface is hinged at the aft of the fuselage, similar in configuration to the Space Shuttle's body flap. Under nominal operations, this surface is used for pitch trim control, but may be used for active pitch control under failures.

Note that although the X-40A is modeled here to include a speedbrake and bodyflap, the actual vehicle is not equipped with these devices. However, the X-37 RLV is equipped with these effectors. The actuator models and the influence of these effectors on the X-40A vehicle dynamics were drawn from the X-37 simulation model. These additional control effectors were included in the demonstration vehicle to allow for more varied failure and reconfiguration studies, and to facilitate transition to the X-37 program.

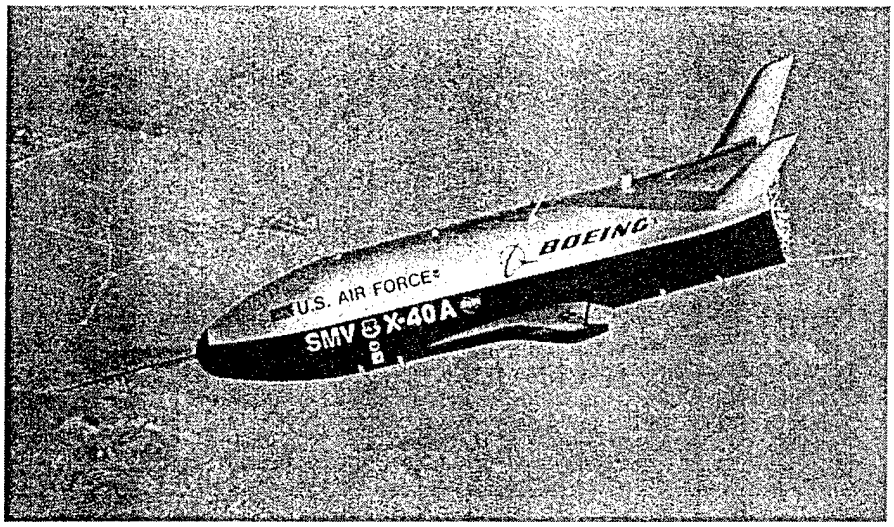

Figure 1. Boeing's X-40A RLV in Drop Tests.

The algorithms developed in this effort were then successfully flight tested under the AFRL-funded Integrated Adaptive Guidance & Control (IAG&C) program. The flight tests were completed by the Flight and Aerospace Research Group, General Dynamics Advanced Information Systems (GDAIS) - formally Veridian – using the Total In-Flight Simulator (TIFS) research aircraft, as shown in Figure 2. The TIFS simulated autonomous approach/landings of the X-40A under a variety of single and multiple control surface failure experiments. The majority of the flight test results indicated the significant benefits of the control reconfiguration, guidance adaptation and trajectory-command reshaping, concluding in successful touchdown conditions. Although most touchdowns were simulated at an altitude of 200 feet, the safety pilots of the TIFS vehicle were comfortable enough with the simulated (unpiloted) system to allow some of the experiments to complete actual touchdowns.

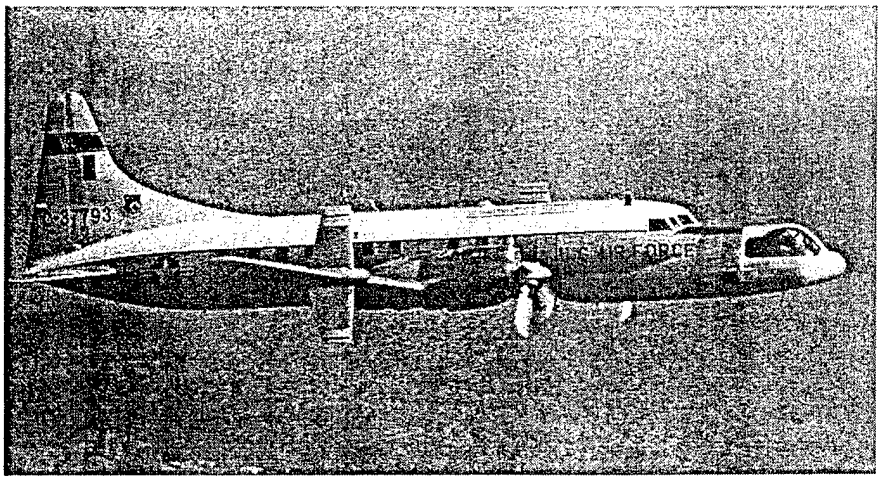

Figure 2. GDAIS's Total In-Flight Simulator (TIFS) Research Aircraft.

The OPTG trajectory command-reshaping algorithm and reconfigurable control system have been presented in detail in [2] and [3], respectively. Details of the adaptive guidance system will be presented next, followed by a brief summary of the OPTG algorithm. Simulation and flight test results will then be presented that show the benefits of the guidance adaptation and trajectory command reshaping.

2. DESIGN OVERVIEW

An overview of the design architecture is given in Figure 3. Again, the inner-loop reconfigurable controller was developed by AFRL. The final design of this controller involved a perfect model-following approach with optimal control allocation to enable control reconfiguration. Again, further details of this design can be found in [3]. The adaptive backstepping guidance law delivers a pitch rate command to the inner-loop control law. Boeing's lateral guidance law was adopted to deliver yaw rate and roll rate commands. The lateral guidance law will not be covered in this paper, as the majority of failure cases experienced little lateral-directional motion, and the main focus of the flight test experiments was on the longitudinal guidance problem. Guidance law feedback gains are adapted depending on whether control surfaces are saturated. Information regarding control surface saturation is obtained form the inner-loop system. Critical parameters are defined as upper and lower bounds on trim lift and drag coefficients. This information is fed to the Optimum Path-To-Go (OPTG) trajectory-reshaping algorithm to determine the appropriate trajectory to follow. The OPTG algorithm then delivers altitude and flight path angle commands to the guidance law.

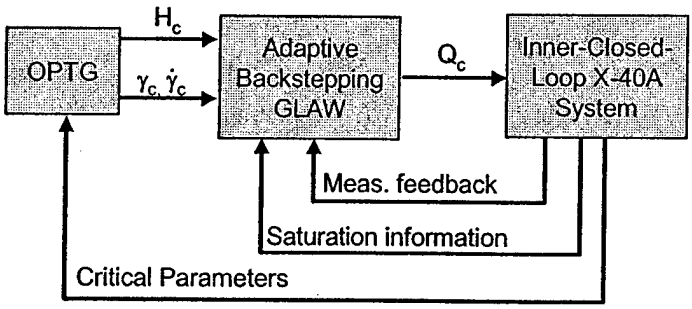

Figure 3. Overview of Design Architecture.

3. X-40A ADAPTIVE GUIDANCE LAW DESIGN

3.1. DESIGN OVERVIEW

Backstepping is a control approach by which "pseudo commands" are generated at each loop closure that drives the next-most inner loop. These commands are derived by dynamic inversion. Consider plant dynamics expressed as,

$$\dot{x} = f(x) + g(u) \tag{1}$$

The objective of dynamic inversion is to generate a control law that "cancels" the plant dynamics and follows a desired state rate, $\dot{x}_{des}$. Dynamic inversion takes on various forms depending on how $\dot{x}_{des}$ is generated, and how plant-modeling errors are dealt with. A fundamental form for a dynamic inversion control law is:

$$u^* = g^{-1}\{\dot{x}_{des} - f(x)\} \tag{2}$$

where g^{-1} is defined such that $g^{-1}(g(u)) = u$.

For fixed-wing aircraft systems such as the X-40A, a natural loop-closure architecture that allows for the backstepping approach is:

i. Altitude loop (outer most loop) to
ii. Flight-path-angle loop to
iii. Angle-of-attack loop (inner-most loop).

The last loop then generates the pitch rate command that drives the inner-closed-loop pitch dynamics. This architecture is depicted in Figure 4 below.

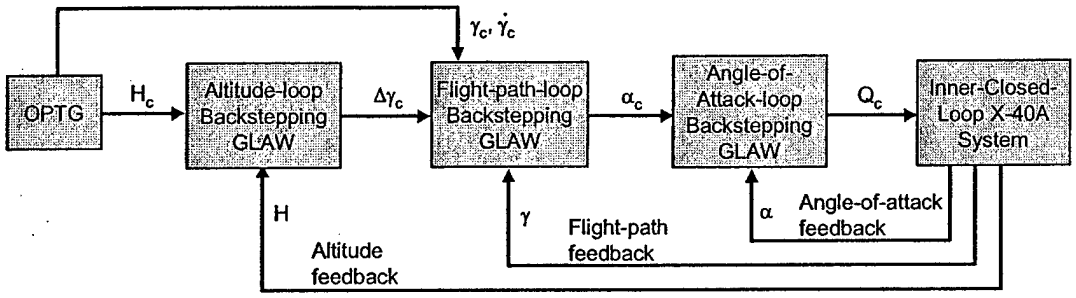

Figure 4. Backstepping Guidance Law Architecture.

3.2. ALTITUDE LOOP GUIDANCE LAW

Using the design paradigm just described, we start with the altitude loop to formulate the appropriate flight-path-angle command. The governing equation of motion here is:

$$\dot{H} = V\sin(\gamma) \tag{3}$$

Defining,

$$\begin{aligned} f_H(H) &\triangleq 0 \\ g_H(\gamma) &\triangleq V\sin(\gamma) \Rightarrow g_H^{-1}(\cdot) = \sin^{-1}(\frac{\cdot}{V}) \end{aligned} \tag{4}$$

Then Eq. (3) may be expressed as

$$\dot{H} = f_H(H) + g_H(\gamma) \tag{5}$$

Therefore, as in Eq. (2), solving for γ, the flight-path-angle command can be derived as:

$$\gamma_c = g_H^{-1}(\dot{H}_{des} - f_H(H)) \tag{6}$$

Substitution of Eq. (4) into Eq. (6) gives

$$\gamma_c = \sin^{-1}(\dot{H}_{des}/V) \tag{7}$$

Note from Figure 4 that the altitude loop backstepping guidance law delivers a corrective flight-path angle command, or $\Delta\gamma_c$. Therefore,

$$\Delta\gamma_c = \sin^{-1}(\Delta\dot{H}_{des}/V) \tag{8}$$

The corrective sink rate command, $\Delta\dot{H}_{des}$, is derived from PI control on altitude error. In the Laplace domain,[1] this can be expressed as,

$$\Delta\dot{H}_{des}(s) = \left(K_H + \frac{K_{H_I}}{s}\right)(H_c(s) - H(s)) \tag{9}$$

where the altitude command, $H_c(s)$ is derived from the OPTG algorithm. From the above equations, the altitude loop backstepping guidance law is depicted in Figure 5.

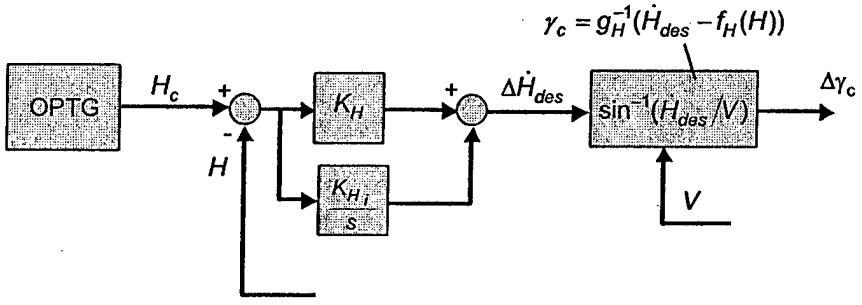

Figure 5. Altitude Loop Backstepping Guidance Law.

3.3. FLIGHT PATH LOOP GUIDANCE LAW

Next, we turn attention to the flight-path-angle loop to formulate the appropriate angle-of-attack command. The governing equation of motion here is:

$$\dot{\gamma} = \frac{L}{mV} - \frac{g}{V}\cos(\gamma) \tag{10}$$

It is assumed here that total vehicle lift, L, can be expressed as follows:

$$L = L_o + L_\alpha\alpha + \{L_\delta\}\vec{\delta} \tag{11}$$

where L_o is lift at zero angle-of-attack, L_α is the dimensional lift-curve slope, $\{L_\delta\}$ is a row vector of lift increment due to each control surface deflection, and $\vec{\delta}$ is the vector of control surface deflection values. Defining

[1] PI control is presented here in the familiar Laplace domain (i.e. for continuous systems) for clarity. However, the actual implementation of the all the algorithms was in the discrete-time domain.

$$L' = L_o + \{L_\delta\}\bar{\delta} \tag{12}$$

then,

$$L = L' + L_\alpha \alpha \tag{13}$$

Substituting Eq. (13) into Eq. (10) gives:

$$\dot{\gamma} = -\frac{g}{V}\cos(\gamma) + \frac{L'}{mV} + \frac{L_\alpha}{mV}\alpha \tag{14}$$

Defining,

$$\begin{aligned} f_\gamma(\gamma) &\triangleq -\frac{g}{V}\cos(\gamma) + \frac{L'}{mV} \\ g_\gamma(\alpha) &\triangleq g_\gamma \alpha = \frac{L_\alpha}{mV}\alpha \Rightarrow g_\gamma^{-1} = \frac{mV}{L_\alpha} \end{aligned} \tag{15}$$

Then Eq. (14) may be expressed as

$$\dot{\gamma} = f_\gamma(\gamma) + g_\gamma \alpha \tag{16}$$

Therefore, as in Eq. (2), solving for α, the angle-of-attack command can be derived as:

$$\alpha_c = g_\gamma^{-1}(\dot{\gamma}_{des} - f_\gamma(\gamma)) \tag{17}$$

Substitution of Eq. (15) into Eq. (17) gives

$$\alpha_c = \frac{mV}{L_\alpha}(\dot{\gamma}_{des} + \frac{g}{V}\cos(\gamma) - \frac{L'}{mV}) \tag{18}$$

PI control is again used to derive the desired flight path angle dynamics. Therefore, the desired flight path angle rate is defined in the Laplace domain as:

$$\dot{\gamma}_{des}(s) = \dot{\gamma}_c(s) + \left(K_\gamma + \frac{K_{\gamma_I}}{s}\right)(\gamma_c(s) + \Delta\gamma_c(s) - \gamma(s)) \tag{19}$$

where the flight path angle and flight path angle rate commands, $\gamma_c(s)$, $\dot{\gamma}_c(s)$, are derived from the OPTG algorithm. Again, the corrective term on the flight path angle command, $\Delta\gamma_c(s)$, is derived from the altitude loop guidance law (see Eq. (8)). From the above equations, the flight-path loop backstepping guidance law is depicted in Figure 6 below.

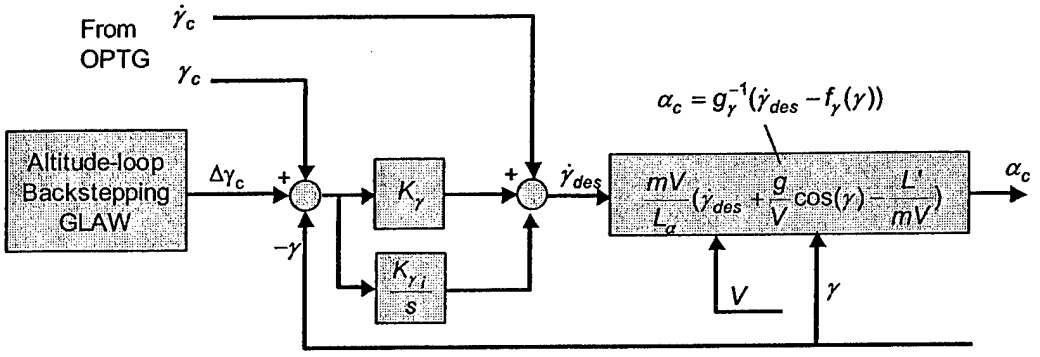

Figure 6. Flight-Path Loop Backstepping Guidance Law.

3.4. INTEGRATOR ANTI-WINDUP LOGIC

Integrator anti-windup logic was added to help preserve stability when saturation occurs in either the angle-of-attack loop or pitch-axis saturation occurs in the inner loop control allocator. The angle-of-attack command is limited between –5 and 24 degrees (the bounds of the aerodynamic database). If the angle-of-attack command needs to exceed this limit in order to track the trajectory, the integrator states will quickly grow due to tracking errors. A similar situation will occur if the inner loop becomes saturated and can no longer achieve the pitch rate command. When either of these situations arises, the integrator states in the altitude and flight-path loops are held at their current values.

3.5. ANGLE-OF-ATTACK LOOP GUIDANCE LAW

Lastly, attention is turned to the angle-of-attack loop to formulate the appropriate pitch rate command for the inner-loop control law. From $\theta = \alpha + \gamma$, and ignoring lateral-directional influences on the pitch rate so that $Q = \dot{\theta}$, the governing equation of motion here is:

$$\dot{\alpha} = -\dot{\gamma} + Q \tag{20}$$

or,

$$\dot{\alpha} = \frac{g}{V}\cos(\gamma) - \frac{L'}{mV} - \frac{L_\alpha}{mV}\alpha + Q \tag{21}$$

Defining,

$$f_\alpha(\gamma,\alpha) \triangleq \frac{g}{V}\cos(\gamma) - \frac{L'}{mV} - \frac{L_\alpha}{mV}\alpha$$
$$g_\alpha(Q) \triangleq Q \Rightarrow g_\alpha^{-1} = 1 \tag{22}$$

Then Eq. (21) may be expressed as

$$\dot{\alpha} = f_\alpha(\gamma,\alpha) + g_\alpha Q \tag{23}$$

Therefore, as in Eq. (2), solving for Q, the pitch rate command can be derived as:

$$Q_c = g_\alpha^{-1}(\dot{\alpha}_{des} - f_\alpha(\gamma,\alpha)) \tag{24}$$

Substitution of Eq. (22) into Eq. (24) gives

$$Q_c = \dot{\alpha}_{des} - \frac{g}{V}\cos(\gamma) + \frac{L'}{mV} + \frac{L_\alpha}{mV}\alpha \tag{25}$$

We seek stable, first order angle-of-attack tracking. Hence, the desired angle-of-attack dynamics are defined as:

$$\dot{\alpha}_{des} = K_\alpha(\alpha_c - \alpha) \tag{26}$$

where α_c is the angle-of-attack command generated from the flight-path loop backstepping guidance law (Eq. (18)). From the above equations, the angle-of-attack loop backstepping guidance law is depicted in Figure 7.

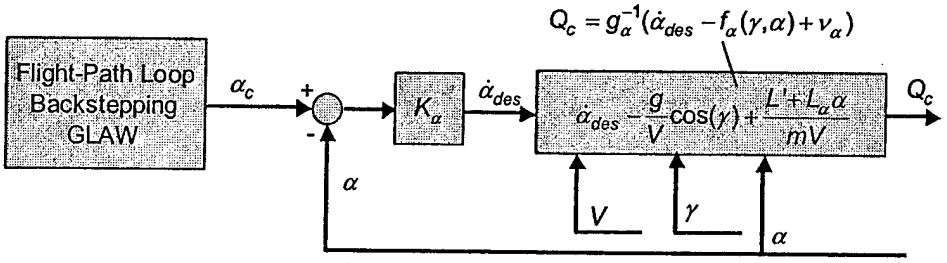

Figure 7. Angle-of-Attack Loop Backstepping Guidance Law.

3.6. GUIDANCE LAW GAIN ADAPTATION

Guidance law gain adaptation was introduced to address control-axis saturation in the inner-loop control allocator. When an axis of the inner loop becomes saturated, the bandwidth of that axis is reduced. This reduction in inner loop bandwidth will erode the stability margins of the outer guidance loops if the same gain values are used. To preserve the stability margins of the backstepping guidance loops, the feedback gains K_H, K_γ and K_α are adapted to account for reductions in the bandwidth of the pitch axis of the inner loop. Currently, the guidance loop gains are factors of the inner-loop bandwidth (see table below). These factors were selected using the Nyquist frequency separation criterion as a guideline.

Table 1. Guidance Loop Gain Adaptation Law.

	Factor of Inner Loop Bandwidth	Nominal Gain Value
Altitude Loop, K_H	1/15	0.2
Gamma Loop, K_γ	1/5	0.6
Alpha Loop, K_α	5/9	1.67

It was found that the guidance loop gain adaptation was not typically necessary for the case studies involved with the flight tests (although high wind gust conditions were seen to cause axis saturation and subsequent guidance adaptation). Therefore, this element of the overall system

was not rigorously tested. Further testing of this adaptation approach may yield more maturation of the design approach, including adaptation of the integrator gains.

3.7. FINAL FLARE GUIDANCE LAW

At an altitude of 150 feet, the backstepping guidance law is turned off, and the final flare guidance law is enabled (or Pmode_4 in Shuttle-heritage guidance law terminology). In this mode, an exponential altitude profile is tracked instead of tracking the trajectory provided by the OPTG algorithm. This profile is generated using a linear relationship between altitude and sink rate, as shown in Figure 8. That is,

$$\dot{H}_c = -\frac{H}{\tau_{ff}} + \dot{H}_{des} \tag{27}$$

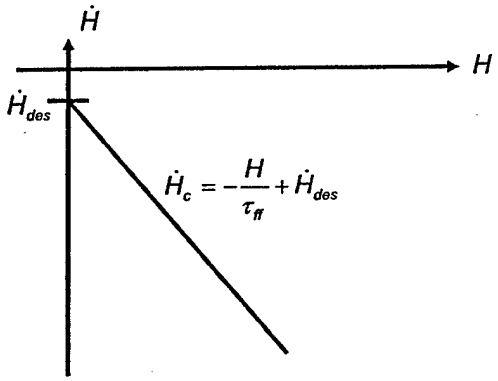

Figure 8. Altitude –vs- Sink Rate Profile During Final Flare Guidance.

By adjusting the time constant τ_{ff} the exponential profile can be made more or less aggressive. The time constant is chosen automatically at the start of the final flare to preserve continuity in the sink rate profile. That is,

$$\tau_{ff} = (150\ ft)/(\dot{H}_{des} - \dot{H}_{@150ft}) \tag{28}$$

In addition to preserving continuity, this scheme selects a more or less aggressive time constant depending on the magnitude of the sink rate at 150 ft.

The sink rate command is converted into a flight path angle command using the same relationship as before, $\gamma_c = sin^{-1}(\dot{H}_c/V)$ (see Eq. (7)). Note, however, there is no longer a corrective term on the flight path angle command (from the altitude loop guidance law) because the primary objective of the final flare guidance is to arrest the sink rate in preparation for landing. Following flight path angle is less important than tracking the desired sink rate profile. This scheme has been found to be robust to disturbances and other variations, consistently achieving touchdown sink rates well within the acceptable limit (-9 fps).

4. X-40A TRAJECTORY COMMAND RESHAPING DESIGN – SUMMARY

The OPTG trajectory-reshaping algorithm is tasked to find a re-targeted trajectory that requires only forces and moments that can be achieved by the degraded capabilities of the vehicle while meeting certain critical constraints. As shown in Figure 4, the re-targeted trajectory is expressed in terms of altitude, flight path angle and flight path angle rate commands. These commands, derived from the on-line OPTG algorithm, drive the guidance loops. The main steps to the OPTG design protocol are listed below.

Off-Line Trajectory Optimization Formulation: For the mission segment under study, a trajectory optimization problem is first formulated by defining the objective function, boundaries of admissible initial/final conditions, admissible variations in critical parameters (again, bounds on trim lift and drag), any particular constraints and the appropriate governing equations of motion. Once properly formulated, candidate trajectories can be readily obtained.

Off-Line Trajectory Database Generation: A database of neighboring extremals is generated by successively varying initial conditions and critical parameters. Such trajectories represent optimal flight paths for the vehicle under failure conditions. Libraries of trajectory databases are generated by repeating this procedure for several downrange locations (usually in equally spaced intervals). This large volume of trajectory data can be cumbersome to interrogate on-line with traditional table lookup methods. The next step in the OPTG approach solves this problem.

Off-Line Trajectory Encoding: This aspect of the OPTG methodology is the most important in terms of enabling on-line use. First, from the set of neighboring extremals found in Step 1, the states of the systems are modeled as a set of selected basis functions most appropriate for the mission segment. Polynomials in downrange have been selected here for the approach-to-landing flight phase, which is largely 2-dimensional flight (vertical plane motion). A nonlinear function-modeling tool is then used to generate polynomial neural networks (PNNs) that map the current vehicle observables (states and critical parameters) to the coefficients of the basis functions describing the associated trajectory. These mappings relate the observables to the basis function coefficients in an efficient, compact manner.

On-Line PNN Interrogation: The final step in the OPTG approach is performed on-line. During flight, the current vehicle states and critical parameters are obtained from measurements or reconstructed from an on-line identification algorithm. This information is then used to compute an appropriate set of basis function coefficients by interrogating the PNNs. Sensor noise and atmospheric disturbances, such as gusts or unpredicted winds, are difficult to include in a trajectory database and thus would not be represented in the PNN models. To be robust to such disturbances and errors, the PNNs are augmented with an on-line coefficient correction algorithm to ensure that the final conditions are met (here, a simple least-squares fit routine has been seen to work quite well). The trajectory commands are then calculated from the corrected basis functions. The loop is closed by re-interrogating the PNNs at regular intervals – typically on the order of 1 Hz. In this manner, trajectories are reshaped in flight to account for changes in the vehicle dynamics due to control surface failures or other significant anomalous events.

5. EXAMPLE HIGH FIDELITY SIMULATION RESULTS

In this section we present an extreme failure case that still resulted in a successful recovery in high-fidelity simulation. The failure was defined as:

Body flap failed at -3 deg. (trailing edge up)
Both left and right ruddervators failed at 0 deg.

In this case, three of the six available control surfaces have failed. The failure occurs at approximately 2.5 nautical miles down range. Figure 9 presents the trajectory profile (altitude – vs- downrange). Plotted are the nominal (no failure) trajectory in the blue solid line, the trajectory for the vehicle with no on-line trajectory reshaping in the red dashed line, and the trajectory for the vehicle with on-line reshaping in the green dashed line. Note that for both cases with and without trajectory reshaping, the inner-loop control reconfiguration and guidance loop adaptation are active. It can be seen that for the case with no reshaping, the vehicle cannot follow the nominal trajectory, and essentially flies straight into the ground. For the case with trajectory reshaping, the vehicle flies a significantly different course. Here, the OPTG algorithm has correctly assigned a commanded trajectory that will not violate the new lift and drag characteristics of the failed vehicle. Figure 10 presents a close-up of the trajectories near touchdown. A smooth main flare to touchdown can be seen for the case with trajectory reshaping.

Figure 11 presents the sink rate history. Here, the touchdown sink rate for the nominal case is approximately –2 fps. For the case with no trajectory reshaping, the touchdown sink rate is approximately –25 fps. This would almost certainly destroy the vehicle. However, the touchdown sink rate for the case with trajectory reshaping is approximately –7 fps, within the acceptable limits of the X-40A. Therefore, even under this very severe failure condition, the vehicle would be able to land without structural damage if it were to possess trajectory-reshaping capabilities.

Figure 12 presents the flight path angle histories. Here, the nominal flight path at touchdown is approximately –1 deg. For the case with no trajectory reshaping, the touchdown flight path angle is approximately –5 deg., and the touchdown flight path angle for the case with trajectory reshaping is approximately –2 deg. Figure 13 presents the angle-of-attack histories. Here, the nominal angle-of-attack at touchdown is approximately 12 deg. For the case with no trajectory reshaping, the touchdown angle-of-attack is significantly high (near the valid limits) at approximately 24 deg., whereas the touchdown angle-of-attack for the case with trajectory reshaping is approximately 15 deg., well within acceptable values. Lastly, Figure 14 presents the true airspeed history. It can be seen that the touchdown velocity for the case with trajectory reshaping is near that of the nominal case, whereas for the case with no trajectory reshaping, the touchdown velocity is significantly higher.

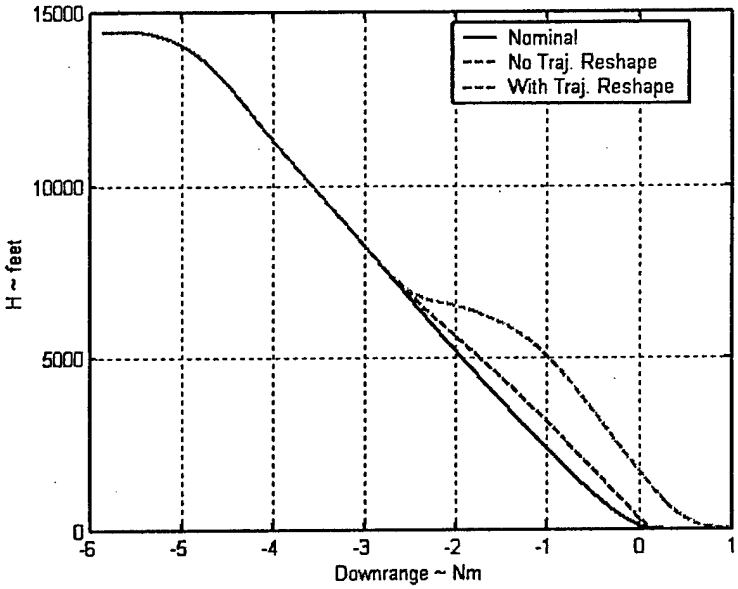

Figure 9. Trajectory Profile – Altitude –vs- Downrange.

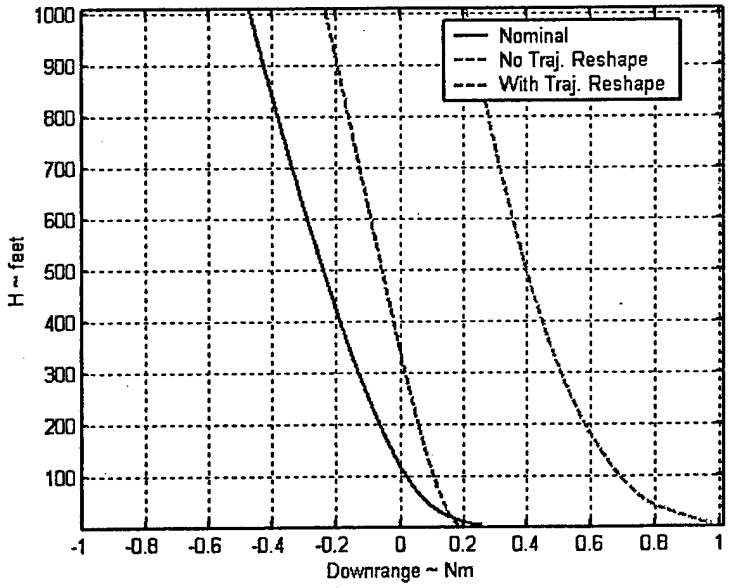

Figure 10. Trajectory Profile Close Up Near Touchdown.

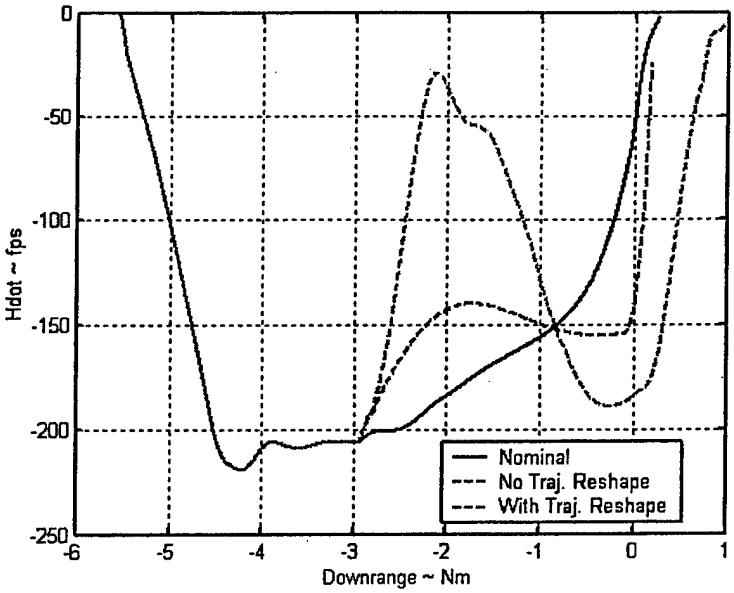

Figure 11. Sink Rate History.

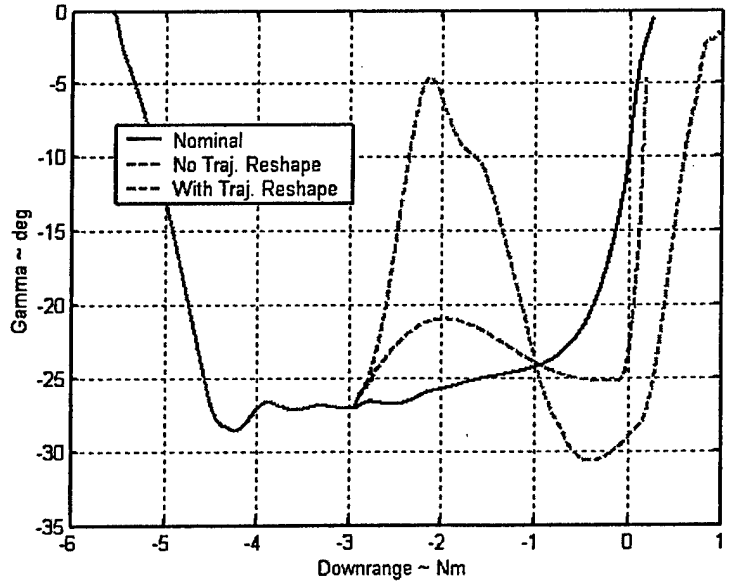

Figure 12. Flight Path Angle History.

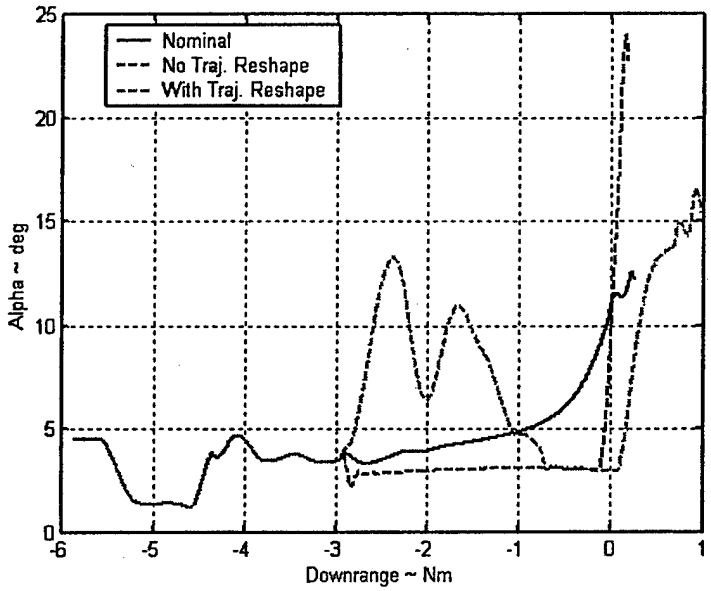

Figure 13. Angle-of-Attack History.

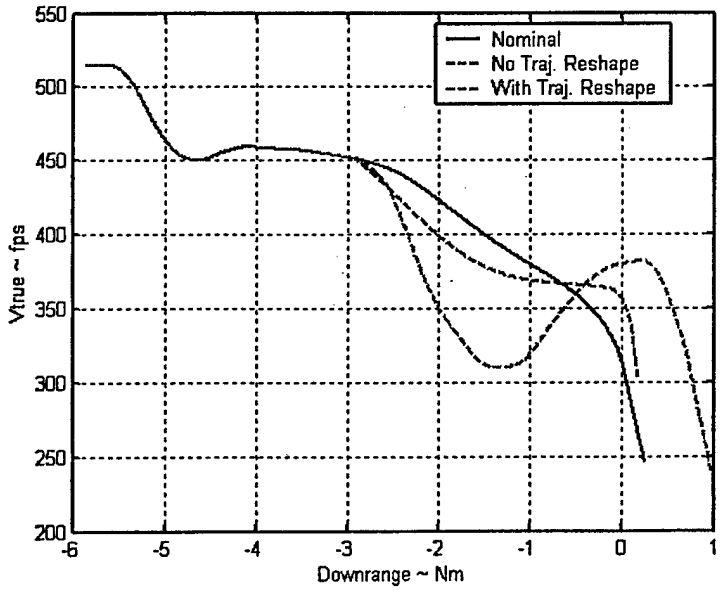

Figure 14. True Airspeed History.

These results were typical for a significant number of failure cases involving different control surfaces or combinations of control surfaces at various failure deflection values.

6. FLIGHT TEST RESULTS

For the final draft of the manuscript, flight test results will be presented. Parameters such as those shown in the previous section will be presented, along with control surface deflection histories for example test cases. Although not shown here, the flight test results were consistent with the batch simulation results and clearly indicated the benefits of the adaptive technologies.

7. CONCLUSIONS

Reconfiguration capabilities will be essential for the success of future autonomous Reusable Launch Vehicles (RLVs). RLVs typically have a minimal set of control effectors, and full recovery of nominal maneuvering capabilities may be physically impossible for a large set of failure scenarios. Because of this, there will be three main elements to RLV reconfiguration: control reconfiguration, guidance adaptation and trajectory reshaping. Final conditions of the mission segment may be unachievable if the trajectory commands driving the guidance loops are not reshaped on-line. However, for the vehicle to successfully follow a reshaped trajectory, it must first be stable in its attitude and flight path motions, which may require both control reconfiguration and guidance gain adaptation.

The focus of the paper was on the adaptive guidance system that worked in conjunction with an autonomous trajectory-reshaping algorithm and a reconfigurable controller. Extensive failure analyses and simulation experiments were performed using a modified version of Boeing's X-40A RLV. The focus of the failure experiments was on the approach-to-landing flight phase. Simulation and flight test results were presented. The results showed that some failure cases will require not only control reconfiguration, but guidance adaptation and trajectory reshaping as well in order for the mission to be recovered.

The flight test effort has resulted in a significant maturation of the guidance and trajectory reshaping technologies, and further developments of these approaches continue.

ACKNOWLEDGEMENTS

This work was funded under two SBIR programs sponsored by (1) the Air Force Research Laboratory, Dr. David Doman, Technical Monitor, and (2) the Marshall Space Flight Center, Mr. Greg Dukeman and Dr. John Hanson, Technical Monitors. *Their support is gratefully appreciated.* Acknowledgments are also due to Boeing, Huntington Beach, which aided in the development of the demonstration model, and to General Dynamics Advanced Information Systems (formally Veridian) for their help and advice in the course of the flight test program.

REFERENCES

1. Sharma, M., "Flight-Path Angle Control via Neuro-Adaptive Backstepping," AIAA-2002-4451, Proc. AIAA Guidance, Navigation, and Control Conf., Monterey, CA, Aug. 2002.

2. Schierman, J., Hull, J., Ward, D., "On-Line Trajectory Command Reshaping for Reusable Launch Vehicles," AIAA-2003-5439, Proc. AIAA Guidance, Navigation, and Control Conf., Austin, TX, Aug. 2003.

3. Oppenheimer, M., Doman, D., "Reconfigurable Inner Loop Control of a Space Maneuvering Vehicle," AIAA-2003-5358, Proc. AIAA Guidance, Navigation, and Control Conf., Austin, TX, Aug. 2003.